An Atomistic-to-Continuum Coupling Method for Heat Transfer in Solids

G.J. Wagner [a,*], R.E. Jones [a], J.A. Templeton [a], M.L. Parks [b]

[a] *Sandia National Laboratories, Livermore, CA 94551*

[b] *Sandia National Laboratories, Albuquerque, NM 87123*

Abstract

In this work, we present a seamless, energy-conserving method to couple atomistic and continuum representations of a temperature field in a material. This technique allows a molecular dynamics simulation to be used in localized regions of the computational domain, surrounded and overlaid by a continuum finite element representation. Thermal energy can pass between the two regions in either direction, making larger simulations of nanoscale thermal processes possible. We discuss theoretical developments and numerical implementation details. In addition, we present and analyze a set of representative simulations.

Key words: atomistic-to-continuum coupling, heat transfer, finite elements, multi-scale simulations

1 Introduction

As technological advances allow the engineering of devices at ever decreasing length scales, and as ever increasing fidelity is demanded in the computational simulation of these devices, it has become clear that traditional material models based on continuum descriptions of solids can be inadequate at the micro- and nano-scales. Surface effects, grain boundaries, defects, and other deviations from a perfect continuum can have a large effect on material behavior at these scales, and simulation techniques based on descriptions at the atom scale, such as molecular dynamics (MD), have become an important part of

* Corresponding author.

Email addresses: gjwagne@sandia.gov (G.J. Wagner), rjones@sandia.gov (R.E. Jones), jatempl@sandia.gov (J.A. Templeton), mlparks@sandia.gov (M.L. Parks).

the computational toolbox. However, molecular dynamics simulations on even the largest supercomputers are currently limited to systems on the order of a billion atoms [1], large enough for the study of some nano-scale phenomena but still far too small to resolve the micro-to-macroscale interactions that must be captured in the simulation of any real device. The recognition of this limitation on MD has led to the development of several methods for the coupling of atomistic and continuum material descriptions in a single simulation; see [2,3] for reviews of these methods. The goal of these methods is to allow the use of a continuum-based technique such as finite elements (FE) in parts of the domain where such a description is valid, while using MD near defects or in other regions in which the continuum description breaks down.

To date, most of these atomistic-to-continuum coupling methods have been based on the coupling of the momentum equation (or in the case of quasi-static problems, the equilibrium equation) in the continuum to the equations of motion for the atoms, usually by combining the Hamiltonians of the two systems [4] or by ensuring that internal forces are properly balanced [5]. Most often, these methods assume that the temperature of the continuum region is in effect zero, and quite a bit of attention has been paid to reducing unwanted internal reflections of waves in the MD lattice at the MD-continuum interface. However, a much more typical scenario for real devices is a temperature that is far above absolute zero. In this case, it is more accurate to recognize lattice waves as energy-carrying phonons, and to think of the surrounding continuum as a thermal bath that maintains the correct balance of incoming and outgoing phonons at the interface at the local temperature.

Some attempts have been made previously to accurately account for the effects of non-zero temperature. Dupuy *et al.* [6] have developed a finite-temperature version of the Quasicontinuum Method that uses a local-harmonic approximation, at a constant temperature, to account for thermal fluctuations of atoms. Rudd and Broughton [7] have developed the coarse-grained molecular dynamics (CGMD) technique for simulations of anharmonic solids at finite temperatures. The bridging scale decomposition method of Wagner and Liu [8] has been extended to finite temperatures by Park *et al.* [9]. However, to our knowledge, no technique exists to couple the thermal fluctuations in the MD region with an energy equation in the continuum to effect true two-way temperature coupling between the MD and continuum regions. In this work, we present a technique for such a coupling, allowing the simulation of nonequilibrium heat transfer between MD and continuum regions of a domain.

Two-way temperature coupling implies that thermal information can pass out of the MD region into the continuum, and that the temperature of the continuum affects the thermal fluctuations of the MD region. The first direction of information flow, from MD to continuum, is important in applications in which phenomena at the atom scale lead to what would be measured in the

laboratory as changes in macroscale temperature. Examples of such phenomena include friction [10], laser heating [11], fracture [12], and plastic failure [13], all of which have been studied using MD or even coupled MD-continuum simulations but without a complete treatment of macroscale temperature interactions. By coupling a continuum energy equation to the atom dynamics, we can simulate temperature changes in the continuum, possibly over large distances, that are caused by these atom-scale phenomena.

At the same time, in a coupled simulation any temperature field that is imposed on the continuum should have an effect on the thermal fluctuations of atoms in the MD region. For example, a macroscale temperature gradient on the continuum should lead to a heat flux through an MD region embedded within it. It is important to capture this behavior correctly in a simulation method, because it is known that structures at the atomic scale such as inclusions or grain boundaries can have a large effect on the thermal conductivity of the material [14]. The ability to do two-way temperature coupling allows the nanostructure of the MD region to have the proper effect on the continuum temperature field.

Several previous authors have coupled MD simulations to a continuum energy equation. Ivanov *et al.* [11] have used a two-temperature model to incorporate the effects of the electron temperature on the dynamics of the atomic nuclei in simulations of laser heating of metal films. Schall *et al.* [15] employed a thermostat acting on the atoms in an MD simulation to enforce the correct thermal conductivity in simulations of metals; this conductivity is otherwise underpredicted by classical MD. Padgett and Brenner [16] used a similar technique to capture the effects of Joule heating in metal nanowires. The principal innovation of the current work is the ability to couple an MD simulation to the temperature field of a continuum that overlaps and surrounds it, such that the two-way coupling of energy between two different domains is effected.

In this work we will use finite elements to solve the heat equation in the continuum. We begin in Section 2 by defining the basic problem to be solved and stating the assumptions used. In Sections 3 and 4, respectively, we derive the forms of the energy equations to be solved in the MD and FE domains; the coupling between the domains follows naturally from our derivation. Time filtering is introduced in Section 5 to reduce fluctuations in the temperature field, and in Section 6 we present some of the details of the numerical implementation of the method. Example problems are presented in Section 7, and we conclude with a discussion in Section 8.

2 Problem Definition

Consider the problem geometry shown in Figure 1. A domain Ω is discretized with a finite element mesh; the outer boundary of the domain is denoted Γ with outward normal vector $\mathbf{n}$. At the same time, an internal portion of the domain Ω_{md} is filled by a set of atoms $\mathcal{A}$. The remaining portion of the domain in which there are no atoms but only finite elements is denoted Ω_{fem}, so that $\Omega_{md} \cup \Omega_{fem} = \Omega$ and $\Omega_{md} \cap \Omega_{fem} = \emptyset$. The boundary between the two subdomains is given by Γ_{md}, with normal vector $\mathbf{n}_{md}$ oriented into the MD region. Note that the entire domain, including Ω_{md}, is discretized with finite elements, so that the atomistic and finite element descriptions co-exist in Ω_{md}. In the following, the vector $\mathbf{X}$ represents the reference coordinates of a given point in Ω.

We are concerned with heat transfer problems in which we can assume that the Fourier heat law holds in Ω_{fem}, where we will rely on a Galerkin finite element solution. The temperature field $T(\mathbf{X}, t)$ evolves according to:

$$\rho c_p \dot{T}(\mathbf{X}, t) = \boldsymbol{\nabla} \cdot \kappa \boldsymbol{\nabla} T(\mathbf{X}, t) \quad \text{in } \Omega_{fem} \tag{1}$$

where ρ, c_p and κ are the density, specific heat, and thermal conductivity of the material (which we assume to be isotropic). Boundary conditions are specified on Γ, and for generality we assume that Γ can be partitioned into a boundary Γ_T on which temperature is prescribed, and a boundary Γ_q on which heat flux is prescribed:

$$T(\mathbf{X}, t) = \bar{T}(\mathbf{X}, t) \quad \text{on } \Gamma_T \tag{2a}$$

$$-\mathbf{n} \cdot \kappa \boldsymbol{\nabla} T(\mathbf{X}, t) = \bar{q}_n(\mathbf{X}, t) \quad \text{on } \Gamma_q \tag{2b}$$

Initial conditions will be discussed in a later section, because they must be defined and applied after we have completely described our coupled system.

In Ω_{md}, we assume that the heat flow and the corresponding dynamics are too complex, in general, to be described by the Fourier heat law. It is in this region, presumably, that we will capture atomic-level effects on the heat transfer; these may include effects of grain boundaries, inclusions, vacancies, dislocations, free surfaces, or any other nanoscale structures that either make a continuum description inappropriate or have a large enough effect on heat transfer as to prevent *a priori* computation of thermal parameters such as conductivity. Region Ω_{md} will be treated using classical molecular dynamics, with atomic forces derived from an interatomic potential. Note that we are considering only phonon heat transport in this region, and that our molecular dynamics cannot represent the electron-mediated heat transfer that dominates in a metal.

For a given atom α, the equations of motion are given in terms of the atomic position $\mathbf{x}_\alpha$ and velocity $\mathbf{v}_\alpha$:

$$\dot{\mathbf{x}}_\alpha = \mathbf{v}_\alpha \tag{3a}$$

$$m_\alpha \dot{\mathbf{v}}_\alpha = \mathbf{f}_\alpha^{md} \equiv -\frac{\partial U^{md}}{\partial \mathbf{x}_\alpha}(\mathbf{x}_\alpha, \mathbf{x}_\beta, ...) \tag{3b}$$

where m_α is the mass of atom α, and $U^{md}(\mathbf{x}_\alpha, \mathbf{x}_\beta, ...)$ is the interatomic potential energy, which is a function of the positions of all atoms. In Section 3, we will discuss implementation details for these molecular dynamics equations and show how they must be augmented to account for heat transfer from the surrounding continuum region.

In our analysis we will make use of integrals over the domain Ω, which require special treatment in Ω_{md}. We define $g(\mathbf{X})$ to be an integrable function over Ω that takes on values at the atom positions $\mathbf{X}_\alpha$. Hence

$$\int_\Omega g(\mathbf{X}) dV = \int_{\Omega_{md}} g(\mathbf{X}) dV + \int_{\Omega_{fem}} g(\mathbf{X}) dV \tag{4}$$

The particular choice made for the evaluation of $g(\cdot)$ over Ω_{md} lies at the heart of the coupling method because through this means atomistic information is upscaled to the continuum. We define

$$\int_{\Omega_{md}} g(\mathbf{X}) dV \equiv \sum_{\alpha \in \mathcal{A}} g_\alpha \Delta V_\alpha \tag{5}$$

where ΔV_α is the volume associated with atom α. In the case where $g(\mathbf{X})$ corresponds to a continuous function or field, $g_\alpha = g(\mathbf{X}_\alpha)$ and Eqn. (5) is a convenient quadrature; but, where g_α is a quantity, such as atomic velocity, defined only at atoms, Eqn. (5) is a means of homogenization.

3 The Atomistic Temperature Field

3.1 Nodes-to-atoms reduction operation

For a system of atoms at equilibrium, the system temperature T can be written [17]:

$$\frac{3}{2} n_a k_B T = \left\langle \sum_{\alpha \in \mathcal{A}} \frac{1}{2} m_\alpha |\mathbf{v}_\alpha|^2 \right\rangle \tag{6}$$

where k_B is Boltzmann's constant and the angle brackets represent an ensemble or time average. Our primary interest in this work is in non-equilibrium systems, so that (6) does not necessarily apply; however, given this expression

it is convenient to define a field T_α at the atoms which, when averaged, gives the correct temperature if the system is at equilibrium (and with zero mean velocity):

$$T_\alpha \equiv \frac{1}{3k_B} m_\alpha |\mathbf{v}_\alpha|^2 \tag{7}$$

It should be noted that there are lower limits to the applicability of Eqn. (6) in terms of number of atoms and the time interval to average over and that other definitions of a local, nonequilibrium temperature exist, see, e.g., [18–21]. However, the existence of an optimum non-equilibrium temperature measure is still a matter of debate and research, see [22].

The development of a coupled atomistic-to-continuum method requires a relationship between this atomistic temperature field and a continuum field defined on the finite element nodes. We begin by defining an interpolated temperature field $T^h(\mathbf{X}, t)$:

$$T^h(\mathbf{X}, t) \equiv \sum_{I \in \mathcal{N}} N_I(\mathbf{X}) \theta_I(t) \tag{8}$$

In this expression, $\mathcal{N}$ is the set of all nodes in the domain, θ_I is a temperature degree of freedom defined on node I, and $N_I(\mathbf{X})$ is the interpolant associated with node I evaluated at $\mathbf{X}$. Note that because $\mathbf{X}$ represents the time-independent reference coordinate of a point, all of the time dependence of of T^h is through the degrees of freedom θ_I. We will use linear finite element shape functions as our interpolants in this paper, but many other choices are possible. The superscript on T^h reflects the fact that the interpolation can be parameterized in terms of some characteristic mesh size h.

Suppose that we are given a set of atomic temperatures defined as in Eqn. (7), along with a set of nodal temperatures θ_I. To relate the two temperature definitions to each other, we can minimize the squared difference between $T^h(\mathbf{X})$ and some temperature field $T(\mathbf{X})$. That is, we minimize

$$\int_\Omega \Big(T(\mathbf{X}) - T^h(\mathbf{X}) \Big)^2 \, dV \tag{9}$$

where integration over the molecular dynamics region of the domain is computed as in (5). Taking the variation with respect to T_h and setting it to zero gives:

$$\int_\Omega \delta T^h T^h dV = \int_\Omega \delta T^h T dV \tag{10}$$

Now assume that T is a field equal to T^h in Ω_{fem} and T_α at the atom positions in Ω_{md}. Explicit use of (5) then gives:

$$\int_\Omega \delta T^h T^h dV = \sum_{\alpha \in \mathcal{A}} \delta T^h(\mathbf{X}_\alpha) T_\alpha \Delta V_\alpha + \int_{\Omega_{fem}} \delta T^h T^h dV \tag{11}$$

The integral over Ω_{fem} can be subtracted from both sides. Given Eqn. (8) and that the variation δT^h is arbitrary, we can derive an equation true for all I:

$$\sum_{J\in\mathcal{M}}\Big(\sum_{\alpha\in\mathcal{A}} N_{I\alpha}N_{J\alpha}\Delta V_\alpha\Big)\theta_J = \sum_{\alpha\in\mathcal{A}} N_{I\alpha}\Delta V_\alpha T_\alpha \tag{12}$$
$$N_{I\alpha} \equiv N_I(\mathbf{X}_\alpha)$$

Here, $\mathcal{M}$ is the set of all nodes J for which $N_J(\mathbf{X}_\alpha) \neq 0$ for some atom α; i.e. the set of nodes whose shape function supports intersect Ω_{md}.

Eqn. (12) gives a matrix equation for the nodal temperatures $\theta_J,\ J \in \mathcal{M}$. In fact, this is a projection of the atom temperature field into the space of finite element shape functions; we note the similarity between this expression and the projection operation defined in [8] for atom displacements and velocities. In our current work, we find it is unnecessary to compute this projection as defined here; instead, we approximate it using a row-sum lumping of the matrix on the left hand side, leading to:

$$\theta_I = \sum_{\alpha\in\mathcal{A}} \hat{N}_{I\alpha}T_\alpha \tag{13}$$
$$\hat{N}_{I\alpha} \equiv \frac{N_{I\alpha}\Delta V_\alpha}{\sum_{\beta\in\mathcal{A}} N_{I\beta}\Delta V_\beta}$$

Specifically, row-sum lumping is a common procedure for approximating a matrix with a diagonal matrix that consists of replacing each row of the matrix with its sum at the diagonal entry, see, e.g., [23, Appendix 8]. Eqn. (13) defines an atoms-to-nodes reduction operation rather than a true projection operation, where the coefficients $\hat{N}_{I\alpha}$ are scaled finite element shape functions.

3.2 Augmented molecular dynamics force

In order to include the effects of the continuum region on the temperature in Ω_{MD}, we augment the force on each atom by a term that is proportional to the velocity of that atom. This form of control is shared by many popular MD thermostat techniques, including the Nose-Hoover [24] and Berendsen [25] thermostats. A similar approach to controlling the energy of an MD simulation has been used by other authors to apply a known heat flux to atoms [26] and to account for coupling between electron and phonon energies in metals [11].

A drag force $\mathbf{f}^\lambda_\alpha$ is defined and added to the standard molecular dynamics force (cf. Eqn. 3b):

$$m_\alpha\dot{\mathbf{v}}_\alpha = \mathbf{f}^{md}_\alpha + \mathbf{f}^\lambda \tag{14}$$

where

$$\mathbf{f}^\lambda = -\frac{m_\alpha}{2}\lambda_\alpha\mathbf{v}_\alpha. \tag{15}$$

The coefficient $m_\alpha/2$ is an arbitrary multiplier that will simplify later results. The parameter λ_α may be different for every atom. Since this parameter is used to model interaction with the continuum, a natural choice is to let this function be interpolated from a set of nodal values λ_I defined on the set of nodes $\mathcal{M}$:

$$\lambda_\alpha(t) = \sum_{I \in \mathcal{M}} N_{I\alpha} \lambda_I(t) \tag{16}$$

The coefficients λ_I can be chosen to enforce conservation of total energy, as derived in the next section.

3.3 Total energy conservation

The total energy of the combined MD-continuum system can be decomposed between the two regions:

$$E^{tot} = E^{md} + E^{fem} \tag{17}$$

The energy of the molecular dynamics region is the sum of the potential and kinetic energies of the atoms:

$$E^{md} = U^{md} + \frac{1}{2} \sum_\alpha m_\alpha |\mathbf{v}_\alpha|^2 \tag{18}$$

while the energy of the finite element region is given by the thermal energy $\rho c_p T^h$ integrated over Ω_{fem}:

$$E^{fem} = \int_{\Omega_{fem}} \rho c_p T^h(\mathbf{X}, t) dV. \tag{19}$$

We will choose the nodal values λ_I such that total energy is conserved throughout the simulation, i.e. $\dot{E}^{tot} = 0$ if no energy is added to the system at the external boundary. The rate of change of the MD energy is

$$\begin{aligned} \dot{E}^{md} &= \dot{U}^{md} + \sum_{\alpha \in \mathcal{A}} m_\alpha (\mathbf{v}_\alpha \cdot \dot{\mathbf{v}}_\alpha) \\ &= \sum_{\alpha \in \mathcal{A}} \frac{\partial U^{md}}{\partial \mathbf{x}_\alpha} \cdot \dot{\mathbf{x}}_\alpha + \sum_{\alpha \in \mathcal{A}} \mathbf{v}_\alpha \cdot (\mathbf{f}_\alpha^{md} + \mathbf{f}_\alpha^\lambda) \\ &= \sum_{\alpha \in \mathcal{A}} \mathbf{v}_\alpha \cdot \mathbf{f}_\alpha^\lambda \end{aligned} \tag{20}$$

where we have used Eqns. (3b) for the definition of $\mathbf{f}_\alpha^{md}$ and (14) for the substitution of $\dot{\mathbf{v}}_\alpha$.

To compute the rate of change on the finite element system, we use Eqn. (1)

with the boundary condition $\bar{q}_n = 0$ on $\Gamma_q = \Gamma$. Then:

$$\begin{aligned}\dot{E}^{fem} &= \int_{\Omega_{fem}} \rho c_p \dot{T}^h dV \\ &= \int_{\Omega_{fem}} \boldsymbol{\nabla} \cdot \kappa \boldsymbol{\nabla} T^h dV \\ &= \int_{\Gamma_{md}} \mathbf{n}_{md} \cdot \kappa \boldsymbol{\nabla} T^h dA \end{aligned} \tag{21}$$

The total energy balance is then:

$$\sum_{\alpha \in \mathcal{A}} \mathbf{v}_\alpha \cdot \mathbf{f}_\alpha^\lambda = -\int_{\Gamma_{md}} \mathbf{n}_{md} \cdot \kappa \boldsymbol{\nabla} T^h dA \tag{22}$$

Physically, this energy balance suggests that the total work done on the MD system by the additional force $\mathbf{f}_\alpha^\lambda$ is equal to the total energy flux out of the FE and into the MD region.

We will choose the nodal values λ_I to satisfy (22); however, the solution to this single scalar equation for the $n_{\mathcal{M}}$ nodes in $\mathcal{M}$ is clearly non-unique. In order to solve for a set of nodal values, we will "localize" the energy balance by multiplying the summand and integrand by the nodal shape function $N_I(\mathbf{X})$:

$$\sum_{\alpha \in \mathcal{A}} N_{I\alpha} \mathbf{v}_\alpha \cdot \mathbf{f}_\alpha^\lambda = -\int_{\Gamma_{md}} N_I \mathbf{n}_{md} \cdot \kappa \boldsymbol{\nabla} T^h dA \tag{23}$$

Note that a solution to (23) also satisfies (22) because of the partition of unity property of the finite element shape functions ($\sum_I N_I(\mathbf{X}) = 1$), as can be seen by summing (23) over I. Although this choice for the localized energy balance is not unique, it will be shown that this form leads to simplifications in the derivation of finite element heat equation.

Substituting Eqns. (15) and (16) into (23), and making use of the definition of atomic temperature (7), gives, after some rearrangement:

$$\sum_{J \in \mathcal{M}} \Big(\sum_{\alpha \in \mathcal{A}} N_{I\alpha} T_\alpha N_{J_\alpha} \Big) \lambda_J = \frac{2}{3k_B} \int_{\Gamma_{md}} N_I \mathbf{n}_{md} \cdot \kappa \boldsymbol{\nabla} T^h dA \tag{24}$$

This system of $n_{\mathcal{M}}$ equations can be solved for λ_I. The numerical computation of the surface integral on the right-hand side of (24) will be discussed in Section 6.2.

4 The Finite Element Heat Equations

In the previous section we related the kinetic energies of the atoms in the MD region to nodal temperatures θ_I. However, in our two-way coupled system the nodal temperatures are also affected by the thermodynamics of the continuum FE region, and we must derive a heat equation valid over the entire domain. We begin with Eqn (11), from which the reduction operation was derived. Taking the time derivative (note that δT^h is not a function of time) and using the Fourier heat equation (1) in Ω_{fem} gives

$$\int_\Omega \delta T^h \dot{T}^h dV = \sum_{\alpha\in\mathcal{A}} \delta T^h(\mathbf{X}_\alpha)\dot{T}_\alpha \Delta V_\alpha + \int_{\Omega_{fem}} \delta T^h \boldsymbol{\nabla}\cdot\frac{\kappa}{\rho c_p}\boldsymbol{\nabla} T^h dV \tag{25}$$

This leads to a matrix equation for the nodal temperatures:

$$\begin{aligned}\sum_{J\in\mathcal{N}}\Big(\int_\Omega N_I N_J dV\Big)\dot{\theta}_J \\ = \frac{2}{3k_B}\sum_{\alpha\in\mathcal{A}} N_{I\alpha}\Delta V_\alpha \mathbf{v}_\alpha\cdot\Big(\mathbf{f}^{md}_\alpha + \mathbf{f}^{\lambda}_\alpha\Big) - \sum_{J\in\mathcal{N}}\Big(\int_{\Omega_{fem}}\boldsymbol{\nabla}N_I\cdot\frac{\kappa}{\rho c_p}\boldsymbol{\nabla}N_J dV\Big)\theta_J \\ - \int_{\Gamma_q} N_I\frac{\bar{q}_n}{\rho c_p}dA + \sum_{J\in\mathcal{N}}\Big(\int_{\Gamma_{md}} N_I\mathbf{n}_{md}\cdot\frac{\kappa}{\rho c_p}\boldsymbol{\nabla}N_J dA\Big)\theta_J\end{aligned} \tag{26}$$

In deriving this equation, we have made use of the atom temperature definition (7); the modified atomic equation of motion (14); the flux boundary condition (2b); the fact that the variation δT^h is zero on Γ_T; the finite element interpolation for T^h and δT^h (8); and the arbitrariness of the nodal variations $\delta\theta_I$ (except on Γ_T).

A further simplification is possible if we make two assumptions: (1) that the atomic volume ΔV_α is uniform over all atoms, and (2) that the specific heat capacity of the system takes the value given by the Dulong-Petit law for a classical solid [17]:

$$c_p = \frac{3k_B}{\rho\Delta V_\alpha} \tag{27}$$

This expression is a consequence of the equipartition theorem for a harmonic solid. Using the localized energy balance from Eqn. (23), the boundary integral over Γ_{md} can be related to the drag force on the atoms:

$$\sum_{J\in\mathcal{N}}\Big(\int_{\Gamma_{md}} N_I\mathbf{n}_{md}\cdot\frac{\kappa}{\rho c_p}\boldsymbol{\nabla}N_J dA\Big)\theta_J = -\frac{1}{3k_B}\sum_{\alpha\in\mathcal{A}} N_{I\alpha}\Delta V_\alpha\mathbf{v}_\alpha\cdot\mathbf{f}^{\lambda}_\alpha \tag{28}$$

Using this result in Eqn. (26) gives:

$$\sum_{J\in\mathcal{N}}\Big(\int_\Omega N_I N_J dV\Big)\dot{\theta}_J = \frac{2}{3k_B}\sum_{\alpha\in\mathcal{A}} N_{I\alpha}\Delta V_\alpha \mathbf{v}_\alpha \cdot \left(\mathbf{f}_\alpha^{md} + \frac{1}{2}\mathbf{f}_\alpha^{\lambda}\right) - \sum_{J\in\mathcal{N}}\Big(\int_{\Omega_{fem}} \boldsymbol{\nabla} N_I \cdot \frac{\kappa}{\rho c_p}\boldsymbol{\nabla} N_J dV\Big)\theta_J - \int_{\Gamma_q} N_I \frac{\bar{q}_n}{\rho c_p} dA \quad (29)$$

It may seem surprising that the boundary integral over Γ_{md} does not completely cancel the $\mathbf{f}_\alpha^{\lambda}$ term on the atoms. Since the boundary integral represents heat flow into the FE-only region while the $\mathbf{f}_\alpha^{\lambda}$ term represents the work done on the MD system, it might be expected that these quantities are equal and opposite. The reason for the discrepancy is that in the combined system heat equation (29), the temperature represents the total internal energy (kinetic plus potential) of the continuum, while in the MD system the temperature represents only the kinetic energy. The Dulong-Petit law (27) assumes equipartition between kinetic and potential energy modes, so that only half of the energy leaving the FE-only region goes into the kinetic energy of the MD system.

Because the boundary Γ_{md} may cut through the interiors of elements, the integral over Ω_{fem} in (29) is difficult to compute numerically in the form given if standard Gaussian integration over the elements is to be used. To allow the computation of this integral, we can use expression (5) to get

$$\int_{\Omega_{fem}} \boldsymbol{\nabla} N_I \cdot \frac{\kappa}{\rho c_p}\boldsymbol{\nabla} N_J dV = \int_\Omega \boldsymbol{\nabla} N_I \cdot \frac{\kappa}{\rho c_p}\boldsymbol{\nabla} N_J dV - \sum_{\alpha\in\mathcal{A}}\left(\boldsymbol{\nabla} N_I \cdot \frac{\kappa}{\rho c_p}\boldsymbol{\nabla} N_J\right)\Big|_\alpha \Delta V_\alpha \quad (30)$$

The integral over Ω can be computed numerically over the elements using standard Gaussian quadrature. In effect, we use the atoms as a set of quadrature points on which to evaluate the integral on Ω_{md}. Note that this is not the same as assuming that the Fourier law is valid in this region; we are simply evaluating the integrand at the atom positions.

With this approximation the final form of the differential equation for the

nodal temperatures is

$$\sum_{J\in\mathcal{N}}\Big(\int_\Omega N_I N_J dV\Big)\dot{\theta}_J$$
$$= \sum_{\alpha\in\mathcal{A}}\left(\frac{2}{3k_B}N_{I\alpha}\mathbf{v}_\alpha\cdot\left(\mathbf{f}_\alpha^{md}+\frac{1}{2}\mathbf{f}_\alpha^{\lambda}\right)+\sum_{J\in\mathcal{N}}\left(\boldsymbol{\nabla}N_I\cdot\frac{\kappa}{\rho c_p}\boldsymbol{\nabla}N_J\right)\Big|_\alpha\theta_J\right)\Delta V_\alpha$$
$$-\sum_{J\in\mathcal{N}}\Big(\int_\Omega\boldsymbol{\nabla}N_I\cdot\frac{\kappa}{\rho c_p}\boldsymbol{\nabla}N_J dV\Big)\theta_J-\int_{\Gamma_q}N_I\frac{\bar{q}_n}{\rho c_p}dA \quad (31)$$

Eqn. (31) together with the modified momentum equation for the atoms (14) and expressions for the drag force (15) and nodal drag coefficients λ_I (24) define our coupled solution scheme. The atom motions affect the finite element solution through the first term on the right-hand side in (31); the finite element solution feeds back into the atomic system through the drag force. Thermal information can therefore flow in both directions.

5 Time-Filtered Coupling

Simulations using (14) and (31) as written lead to time fluctuations in the nodal temperature field in Ω_{md}. Because they are incompatible with the usual behavior of a continuum that obeys the Fourier heat law, these fluctuations are undesirable if we are trying to couple to a smoothly varying temperature field in the surrounding continuum, or if we want to compare to experimentally measured temperatures. Fluctuations can be reduced by using large elements that effectively average the atomic contributions T_α to the temperature over a large number of atoms. To reduce the fluctuations even further, especially when geometry or other considerations, such as resolving spatial inhomogeneities, prevent use of very large elements, we can average in time. Since this time average is to be computed "on the fly" and used in the coupling scheme, we must use a one-sided, causal time average based only on the past values of the nodal temperature field.

To accomplish this, we define a time filtering operation as:

$$\langle f(t)\rangle \equiv \int_{-\infty}^{t} f(t')G(t-t')dt' \quad (32)$$

where $G(t)$ is a kernel function of the form

$$G(t) = \frac{1}{\tau}e^{-t/\tau} \quad (33)$$

and τ is the time scale of our filtering operation. The filter defined in (32) has

at least three useful properties. First, it commutes with time differentiation:

$$\frac{d}{dt}\langle f\rangle = \left\langle \frac{df}{dt} \right\rangle \tag{34}$$

Second, the time derivative of a filtered function can be rewritten as a simple, first order ODE:

$$\frac{d}{dt}\langle f\rangle = \frac{f - \langle f\rangle}{\tau} \tag{35}$$

so that $\langle f\rangle$ can be obtained by evolving this ODE in time, rather than explicitly calculating the integral in (32). Third, the filter is invertible:

$$\langle f(t)\rangle = g(t) \Rightarrow f(t) = g(t) + \tau\frac{dg}{dt}(t) \tag{36}$$

The first of these three properties is true for any kernel function $G(t)$ that goes to zero as t goes to infinity, but the second and third properties are dependent on our particular choice of $G(t)$.

In order to smooth the fluctuations in the nodal temperature field, we can apply the time filtering operation directly to the atomic temperatures in Eqn (11), giving:

$$\int_\Omega \delta T^h T^h dV = \Big\langle \sum_{\alpha\in\mathcal{A}} \delta T^h(\mathbf{X}_\alpha) T_\alpha \Delta V_\alpha \Big\rangle + \int_{\Omega_{fem}} \delta T^h T^h dV \tag{37}$$

The reduction operation that gives the nodal temperature field in terms of the temperature at the atoms (13) becomes

$$\theta_I = \Big\langle \sum_{\alpha\in\mathcal{A}} \hat{N}_{I\alpha} T_\alpha \Big\rangle \tag{38}$$

The total energy to be conserved (cf. 17) is, in this case,

$$E^{tot} = \langle E^{md}\rangle + E^{fem} \tag{39}$$

Following the same procedure as in Sections 3.2 and 3.3, while applying the filter inversion from (36), gives a slightly different expression for the nodal drag force coefficients (cf. 24):

$$\sum_{J\in\mathcal{M}} \Big(\sum_{\alpha\in\mathcal{A}} N_{I\alpha} T_\alpha N_{J_\alpha} \Big) \lambda_J = \frac{2}{3k_B} \int_{\Gamma_{md}} N_I \mathbf{n}_{md} \cdot \kappa(\boldsymbol{\nabla} T^h + \tau \boldsymbol{\nabla} \dot{T}^h) dA \tag{40}$$

The atomic momentum equations (14), (15), and (16) are otherwise unchanged.

Finally, the finite element temperature evolution equation with time filtering

becomes

$$\sum_{J\in\mathcal{N}}\Big(\int_\Omega N_I N_J dV\Big)\dot{\theta}_J$$
$$= \left\langle \frac{2}{3k_B}\sum_{\alpha\in\mathcal{A}} N_{I\alpha}\mathbf{v}_\alpha \cdot \left(\mathbf{f}_\alpha^{md} + \frac{1}{2}\mathbf{f}_\alpha^{\lambda}\right)\Delta V_\alpha \right\rangle + \sum_{J\in\mathcal{N}}\sum_{\alpha\in\mathcal{A}}\left(\boldsymbol{\nabla} N_I \cdot \frac{\kappa}{\rho c_p}\boldsymbol{\nabla} N_J\right)\Big|_\alpha \theta_J \Delta V_\alpha$$
$$- \sum_{J\in\mathcal{N}}\Big(\int_\Omega \boldsymbol{\nabla} N_I \cdot \frac{\kappa}{\rho c_p}\boldsymbol{\nabla} N_J dV\Big)\theta_J - \int_{\Gamma_q} N_I \frac{\bar{q}_n}{\rho c_p} dA \quad (41)$$

The filtered quantity on the right-hand side is computed at nodes using the ODE in Eqn. (35); this will be more fully described in Section 6.3. Note that in taking the time derivative of Eqn. (38) in order to derive this equation (41), we have used the fact that commutation of filtering and differentiation (34) allows us to move the time derivative inside the filter.

6 Numerical Implementation Details

6.1 Computation of interatomic forces

The force $\mathbf{f}_\alpha^{md}$ on each atom is computed in the standard way for a molecular dynamics simulation, i.e. from the derivative of an interatomic potential function with respect to $\mathbf{x}_\alpha$. In general, this potential depends on interaction between atoms within some specified cutoff radius r_c of each other. One issue that requires special treatment in our coupled method is the handling of atoms within a distance r_c of the boundary Γ_{md}. These atoms do not have the full complement of neighbors that they would have in a bulk solid, and so, if not treated carefully, these atoms will behave as if they are near a free surface rather than in the interior of the domain.

Our approach to handling these atoms is to store the positions of a number of "ghost atoms" located near the boundary Γ_{md}. In this commonly employed treatment, all atoms in the lattice that are within a distance r_c outside the boundary are stored as ghost atoms (see Figure 2). These atoms are considered to be part of the continuum region and thus have zero displacement, but their positions are used to compute the forces in atoms lying on the interior of Ω_{md}.

6.2 Surface integrals on the MD interface

Akin to the issue of evaluating the domain integral over Ω_{fem} in Eqn. (30) , the integral over surface Γ_{md} on the right-hand side of Eqn. (24) may be difficult

to compute especially if the surface does not coincide with finite element faces. We have found that an effective approach is to approximate this integral using a combination of the divergence theorem together with projection of derivative fields onto nodal variables. First, note that the integral in question can be rewritten in terms of volume integrals over Ω_{md}:

$$\int_{\Gamma_{md}} N_I \mathbf{n}_{md} \cdot \kappa \boldsymbol{\nabla} T^h dA = \int_{\Omega_{md}} N_I \boldsymbol{\nabla} \cdot \kappa \boldsymbol{\nabla} T^h dV + \int_{\Omega_{md}} \boldsymbol{\nabla} N_I \cdot \kappa \boldsymbol{\nabla} T^h dV \quad (42)$$

Volume integrals over Ω_{md} can be computed through a sum over atoms, as in Eqn. (5). The difficulty is that the second derivative of T^h, in the first integral on the right-hand side, is infinite on element boundaries when finite element shape functions with standard C^0 continuity are used. However, this integral cannot be neglected, nor simply evaluated on element interiors, since the integral over the element boundaries makes a finite contribution to the total value of the expression. The approach we have taken is to approximate this integral by projecting the second derivative of the temperature onto a field $L(\mathbf{X})$ that is defined by a nodal interpolation:

$$L(\mathbf{X}) = \sum_{I \in \mathcal{N}} N_I(\mathbf{X}) L_I \approx \boldsymbol{\nabla} \cdot \kappa \boldsymbol{\nabla} T^h \quad (43)$$

This leads to an approximation for the values L_I:

$$\begin{aligned} L_I &= \Delta V_I^{-1} \int_{\Omega} N_I \boldsymbol{\nabla} \cdot \kappa \boldsymbol{\nabla} T^h dV \\ &= -\Delta V_I^{-1} \int_{\Omega} \boldsymbol{\nabla} N_I \cdot \kappa \boldsymbol{\nabla} T^h dV - \Delta V_I^{-1} \int_{\Gamma} N_I \bar{q}_n dA \end{aligned} \quad (44)$$

where $\Delta V_I = \int_\Omega N_I dV$ is a measure of the volume associated with node I. In the second line of (44), the boundary integral on Γ is zero as long as node I does not lie on Γ.

With this approximation, the expression for the boundary integral becomes:

$$\begin{aligned} \int_{\Gamma_{md}} N_I \mathbf{n}_{md} \cdot \kappa \boldsymbol{\nabla} T^h dA = \sum_{J \in \mathcal{N}} \left[\int_{\Omega_{md}} N_I N_J dV \right] L_J \\ + \sum_{J \in \mathcal{N}} \left[\int_{\Omega_{md}} \boldsymbol{\nabla} N_I \cdot \kappa \boldsymbol{\nabla} N_J dV \right] \theta_J \end{aligned} \quad (45)$$

Both integrals over Ω_{md} are evaluated by summing over the atoms as in (5). The terms in brackets are constant in time and can be computed at the beginning of the simulation. This approximation for the boundary integral term in Eqn. (24) can be evaluated in the same way whether the MD/FE boundary coincides with element faces or cuts through element interiors; there is no need to store any discretized representation of the surface.

6.3 Time Integration

In order to simplify the description of our time integration scheme, we can rewrite the differential equations (14) and (41) in a more compact form:

$$\dot{\mathbf{x}}_\alpha = \mathbf{v}_\alpha \tag{46a}$$

$$\dot{\mathbf{v}}_\alpha = \frac{1}{m_\alpha}\mathbf{f}_\alpha^{md}(\mathbf{x}_\beta) - \frac{1}{2}\mathbf{v}_\alpha\lambda_\alpha(\mathbf{x}_\beta, \mathbf{v}_\beta, \dot{\theta}_K, \ddot{\theta}_K) \tag{46b}$$

$$\sum_J M_{IJ}\dot{\theta}_J = F_I(\mathbf{x}_\beta, \mathbf{v}_\beta, \theta_K) \tag{46c}$$

where $\beta \in \mathcal{A}$ and $K \in \mathcal{N}$, M_{IJ} is the matrix with elements defined by the integral on the left-hand side of (41), $F_I(\mathbf{x}_\beta, \mathbf{v}_\beta, \theta_K)$ is the right-hand side of (41), and

$$\lambda_\alpha \equiv \sum_{I\in\mathcal{M}} \hat{N}_{I\alpha}\lambda_I \tag{47}$$

Here, the nodal values λ_I are given by the solution to (40). In (46) we have emphasized the dependence of $\mathbf{f}_\alpha^{md}$, λ_α, and F_I on the atomic and nodal variables.

For compactness we will drop subscripts α and I in the following; subscripts will instead represent the timestep as we integrate from step n to step $n+1$. The integration scheme we use is an explicit predictor-corrector method that is second-order accurate in the displacements. The scheme is based on a modified version of the velocity-Verlet algorithm for $\mathbf{x}$ and $\mathbf{v}$ [27], and the Gear predictor-corrector method for θ [28]. First, update the atomic velocities to the half time step $n+\frac{1}{2}$:

$$\tilde{\mathbf{v}}_{n+1/2} = \mathbf{v}_n \exp\Big(-\frac{1}{4}\Delta t\lambda(\mathbf{x}_n, \mathbf{v}_n, \dot{\theta}_n, \ddot{\theta}_n)\Big) \tag{48a}$$

$$\mathbf{v}_{n+1/2} = \tilde{\mathbf{v}}_{n+1/2} + \frac{1}{2m}\Delta t\, \mathbf{f}^{md}(\mathbf{x}_n) \tag{48b}$$

The exponential term in (48a) results from an operator split on (46b), and approximating λ as a constant for a half timestep. The positions can then be updated over the entire time step:

$$\mathbf{x}_{n+1} = \mathbf{x}_n + \Delta t\mathbf{v}_{n+1/2} \tag{49}$$

The predictor step for the nodal temperature field θ_I uses a Taylor expansion about the current state. We find that to retain accuracy when time filtering

is used, we need to store derivatives up to the third derivative $\dddot{\theta}$:

$$\tilde{\theta}_{n+1} = \theta_n + \Delta t\dot{\theta}_n + \frac{1}{2}\Delta t^2\ddot{\theta}_n + \frac{1}{6}\Delta t^3\dddot{\theta}_n \tag{50a}$$

$$\dot{\tilde{\theta}}_{n+1} = \dot{\theta}_n + \Delta t\ddot{\theta}_n + \frac{1}{2}\Delta t^2\dddot{\theta}_n \tag{50b}$$

$$\ddot{\tilde{\theta}}_{n+1} = \ddot{\theta}_n + \Delta t\dddot{\theta}_n \tag{50c}$$

$$\dddot{\tilde{\theta}}_{n+1} = \dddot{\theta}_n \tag{50d}$$

The velocity corrector updates $\mathbf{v}$ to step $n+1$, again using a split operator:

$$\tilde{\mathbf{v}}_{n+1} = \mathbf{v}_{n+1/2} + \frac{1}{2m}\Delta t\mathbf{f}^{md}(\mathbf{x}_{n+1}) \tag{51a}$$

$$\mathbf{v}_{n+1} = \tilde{\mathbf{v}}_{n+1}\exp\Big(-\frac{1}{4}\Delta t\lambda(\mathbf{x}_{n+1}, \tilde{\mathbf{v}}_{n+1}, \dot{\tilde{\theta}}_n, \ddot{\tilde{\theta}}_n)\Big) \tag{51b}$$

Finally, temperature is updated to $n+1$ by computing the correct value of $\dot{\theta}$ from Eqn. (46c):

$$R \equiv \Delta t\Big(M^{-1}F(\mathbf{x}_{n+1}, \mathbf{v}_{n+1}, \tilde{\theta}_{n+1}) - \dot{\tilde{\theta}}_{n+1}\Big) \tag{52a}$$

$$\theta_{n+1} = \tilde{\theta}_{n+1} + \frac{3}{8}R \tag{52b}$$

$$\dot{\theta}_{n+1} = \dot{\tilde{\theta}}_{n+1} + \frac{1}{\Delta t}R \tag{52c}$$

$$\ddot{\theta}_{n+1} = \ddot{\tilde{\theta}}_{n+1} + \frac{3}{2\Delta t^2}R \tag{52d}$$

$$\dddot{\theta}_{n+1} = \dddot{\tilde{\theta}}_{n+1} + \frac{1}{\Delta t^3}R \tag{52e}$$

Coefficients on the right-hand side of Eqn (52) are obtained from Gear [28].

When time filtering is used, filtered values such as the first term on the right-hand side of (41) must be computed. This is done by using the ODE given in (35) to update at every time step. For this we use a simple second-order Crank-Nicholson method; the update of the filtered value of a general function f is the solution to

$$\frac{1}{\Delta t}\Big[\langle f\rangle_{n+1} - \langle f\rangle_n\Big] = \frac{1}{2\tau}\Big[(f_{n+1} - \langle f\rangle_{n+1}) + (f_n - \langle f\rangle_n)\Big] \tag{53}$$

This is easily solved for $\langle f\rangle_{n+1}$. The actual choice of time filter scale τ depends on the size of the mesh elements (i.e. the number of atoms contributing to each nodal temperature) and the acceptable fluctuation sizes; effects of various choices for τ for different meshes on fluctuations are explored in the example in Section 7.1.

Algorithm 1 Time integration algorithm for N total timesteps

initialize temperature θ_0 and its time derivatives at all nodes, and initialize position $\mathbf{x}_0$ and velocity $\mathbf{v}_0$ at all atoms (see Section 6.4)
initialize interatomic forces $\mathbf{f}^{md}(\mathbf{x}_0)$, (Eqn. 3b)
for $n = 0$ to $N - 1$ **do**
  predictor
    solve for thermostat variable $\lambda = \lambda(\mathbf{v}_n, \theta_n, \dot{\theta}_n)$, (Eqn. 40)
    update $\tilde{\mathbf{v}}_{n+1/2} = \mathbf{v}_n \exp\left(-\frac{1}{4}\Delta t \lambda\right)$, (Eqn. 48a)
    Verlet update $\mathbf{v}_{n+1/2} = \tilde{\mathbf{v}}_{n+1/2} + \frac{1}{2m}\Delta t\, \mathbf{f}^{md}(\mathbf{x}_n)$, (Eqn. 48b)
    Verlet update $\mathbf{x}_{n+1} = \mathbf{x}_n + \Delta t\, \mathbf{v}_{n+1/2}$, (Eqn. 49)
    predict temperature $\tilde{\theta}_{n+1}, \dot{\tilde{\theta}}_{n+1}, \ldots$ via Gear formula (Eqn. 50)
  end predictor
  corrector
    compute new interatomic forces $\mathbf{f}^{md}(\mathbf{x}_{n+1})$, (Eqn. 3b)
    set forces on all fixed ghost atoms to zero
    Verlet update $\tilde{\mathbf{v}}_{n+1} = \mathbf{v}_{n+1/2} + \frac{1}{2m}\Delta t\, \mathbf{f}^{md}(\mathbf{x}_{n+1})$, (Eqn. 51a)
    solve for new thermostat variable $\lambda = \lambda(\tilde{\mathbf{v}}_{n+1}, \tilde{\theta}_{n+1}, \dot{\tilde{\theta}}_n))$, (Eqn. 40)
    update $\mathbf{v}_{n+1} = \tilde{\mathbf{v}}_{n+1} \exp\left(-\frac{1}{4}\Delta t \lambda\right)$, (Eqn. 51b)
    compute coupling term in angle brackets in Eqn. (41), and its time-filtered value (Eqn. 53)
    compute $\dot{\theta}_{n+1}$ from energy balance (Eqn. 41)
    correct temperature $\theta_{n+1}, \ddot{\tilde{\theta}}_{n+1}, \ldots$ via Gear formula (Eqn. 52)
  end corrector
  set $n \to n + 1$
end for

A step-by-step summary of the time integration procedure is given in Algorithm 1. Note that in our approach to the time integration, we use the same time step size for both the continuum and MD solutions, although in principal subcycling could be used to take advantange of the fact that the characteristic time scale of the continuum region is longer. In practice, we find that the computational time for the continuum solution is fast compared with the MD update, so there is not a significant advantage to be gained by subcycling, at least for the problem sizes we have run.

6.4 Initial Conditions and the Rescaling Thermostat

In most simulations we require that the initial temperature field at time $t = 0$ in the entire domain be set to some known function. Usually this is a constant value on the domain, although in some cases we desire a spatially varying temperature field. For the finite element temperature field this is simply a matter of setting the nodal values θ_I equal to the desired values at $t = 0$, but

in the MD region we must ensure that the atomic temperatures are consistent with these values, i.e. by Eqn. (13) we require:

$$\sum_{\alpha \in \mathcal{A}} \hat{N}_{I\alpha} T_\alpha = \bar{\theta}_I \tag{54}$$

where $\bar{\theta}_I$ are the desired nodal temperatures.

The state of the system at $t = 0$ must satisfy (54) while still reflecting a reasonable distribution of particle velocities and positions; for example, the total energy should be partitioned approximately equally between potential and kinetic energies. For this reason, we cannot simply assign velocities to the atoms at $t = 0$, but must allow the simulation to achieve a near-equilibrium distribution while enforcing (54), at least on average. One way to achieve this is to evolve the free system dynamics while repeatedly rescaling the atomic velocities by some multiplicative factor $\xi(x)$, which we must compute. Since we want to satisfy the constraint at each node, it seems reasonable to expect that $\xi(x)$ will belong to a function space with a number of degrees of freedom equal to the number of nodes (so that the number of equations will equal the number of unknowns). We will assume therefore that, like θ, ξ is a "coarse" scale variable defined by a set of nodal values ξ_I. We can then obtain ξ at any atom α using our finite element shape functions:

$$\xi_\alpha = \sum_I N_{I\alpha} \xi_I. \tag{55}$$

The rescaled velocity at atom α can then be written:

$$\tilde{\mathbf{v}}_\alpha = \xi_\alpha^{1/2} \mathbf{v}_\alpha. \tag{56}$$

We use the square root of ξ_α to scale the velocity so that when we compute the temperature, which is proportional to v_α^2, the scaling will be linear. After rescaling, the atom velocities satisfy the equation:

$$\sum_I \hat{N}_{I\alpha} \tilde{T}_\alpha = \bar{\theta}_I \tag{57}$$

where

$$\begin{aligned} \tilde{T}_\alpha &= \frac{1}{3k_B} m_\alpha \left| \tilde{\mathbf{v}}_\alpha \right|^2 \\ &= \xi_\alpha T_\alpha \end{aligned} \tag{58}$$

Substituting for the interpolated values of ξ_α gives a simple matrix equation for the nodal values ξ_I:

$$\mathbf{M}^\xi \boldsymbol{\xi} = \bar{\boldsymbol{\theta}} \tag{59}$$

where

$$M^\xi_{IJ} = \sum_\alpha \hat{N}_{I\alpha} T_\alpha N_{J\alpha} \tag{60}$$

Given a set of atomic velocities and an initial temperature field $\bar{\theta}_I$ at time $t = 0$, we can solve for ξ_I, interpolate to the atoms, and rescale the velocities. The resulting atomic temperature field reduced to the nodes will match the given field. In practice, we find that the best initial condition is obtained by allowing the MD system to run freely for a few picoseconds, while periodically applying the rescaling thermostat derived above. This allows time for the system to achieve equipartition of energy between kinetic and potential energies; this equipartition can be imperfect if the rescaling thermostat is applied to a system that is far from the desired temperature or far from equilibrium.

7 Examples

We performed a set of representative problems to investigate and illustrate the performance of the proposed coupling algorithm. All simulations used the Lennard-Jones pair potential

$$\phi(r) = 4\varepsilon\Big(\Big(\frac{\sigma}{r}\Big)^{12} - \Big(\frac{\sigma}{r}\Big)^{6}\Big) \tag{61}$$

for the interatomic interactions with parameters $\varepsilon/k_B = 119.8\,K$ and $\sigma = 3.405\,\mathring{A}$ for solid argon, taken from [29]. Non-periodic atomic boundaries were padded with two unit cells (four layers) of ghost atoms. An atomic mass of $m_\alpha = 39.948\,amu$ was used and the equilibrium, face-centered cubic lattice constant $\ell = 5.406\,\mathring{A} \approx 1.775\sigma$ at $30\,K \approx 0.25\epsilon/k_B$ was calculated using a finite-temperature, zero pressure simulation. The continuum thermal diffusivity $\frac{\kappa}{\rho c_p} = 50\,\mathring{A}^2/ps$ was calculated using a thermal conductivity value $\kappa = 0.5\,W/(mK)$ estimated from [29] and a heat capacity value $\rho c_p = 1.1\,MJ/(Km^3)$ from Eqn. (27). Standard 8-node tri-linear hexahedral elements were employed in the finite element representation of the material.

To initialize the states of the atoms in all of the following simulations, we used the thermostat described in Section 6.4 in a thermalization procedure consisting of rescaling every 100 steps for several thousand time steps. We found that a time step of $0.005\,ps \approx 172.5\,t_E$, was sufficiently accurate and stable to produce the following results. Here, $t_E \approx 0.4\sqrt{m_\alpha\sigma^2/\epsilon}$ is the approximate Einstein vibrational period for the lattice.

7.1 One Dimensional Heat Conduction

In this example, a transient, non-equilibrium heat flux simulation was effected using temperature boundary conditions on the ends of a FE grid which subsumed the MD region. The atomic system was $(20\times8\times8)\ell$ in size and centered

in the overlapping finite element domain of size $(48 \times 8 \times 8)\ell$. The domain was discretized using cubical elements; simulations were run with element sizes of $h = \{8, 4, 2\}\ell$, resulting in meshes with 6, 48, and 384 elements, respectively. The [100] crystal directions were aligned with the axes of the computational domain. The problem geometry for the $h = 4\ell$ case is shown in Figure 3.

Periodic boundaries were imposed on the lateral ($\pm y$ and $\pm z$) faces of the rectangular domain. The temperature of the entire system was initially brought to $30\,K$ via rescaling and, immediately following the thermalization stage, the end temperatures were changed to $40\,K$ and $20\,K$ for the left ($-x$) and right ($+x$) ends, respectively. The longitudinal temperature traces, Figure 4, of this essentially one-dimensional problem show good agreement with the corresponding solution of the classical heat conduction equation. For moderately sized MD simulations, including this simple test problem, we do not expect discernible effects of the finite speed of propagation of heat waves and, consequently, the Fourier model in the FE-only regions appears to be sufficiently representative. The work of Volz *et al.* [30] and Ho *et al.* [31] illustrate, for nearly 1D and strictly 2D systems respectively, the potential discrepancies between Fourier behavior and MD simulations, albeit at much higher pressures and temperatures than those investigated here. Using the estimate $1/\sqrt{3}c_1$ employed in both [30] and [31] for the speed of the "second sound" wave, where c_1 is the speed of the first (transverse) wave, we calculate a thermal wave speed of $c_2 \approx 700\,m/s$. At this velocity a thermal pulse will transit a typical finite element ($h = 4\ell$) in about $3.2\,ps$. Since this transit time is on the order of the filter scale we employ, it is reasonable that our simulations show results that are consistent with a (nearly) infinite speed of heat propagation.

Specifically, we ran simulations using various values of the time filter parameter $\tau = \{0.05, 0.2, 1.0, 5.0, 10.0, 25.0\}\,ps$. As a demonstration of the effect of time filtering on temperature fluctuations, Figure 5 shows the root mean square (RMS) fluctuation in time at the center point of the system as a function of τ for each mesh size h. For large values of τ, the RMS values are proportional to $\tau^{-1/2}$; this is the expected behavior if the number of phonons being averaged over is proportional to the filter time, since the RMS of N samples is expected to be inversely proportional to the square root of N. Likewise, the dependence on the mesh size approximately follows the trend $h^{-3/2}$, consistent with averaging over a number of phonons proportional to the element volume. Note that data was only sampled in the range $t \in [500, 1000]\,ps$, where the temperatures have reached a statistical steady-state.

7.2 Diffusion of an Initial Gaussian Temperature Profile

In order to show consistency between a full MD solution and a coupled simulation, we compared two simulations: (a) a "reference" simulation where the computational region $(32 \times 32 \times 8)\ell$ was completely filled with atoms and the FE grid was only used for data-processing; and (b) a coupled simulation where the MD region $(16\times16\times8)\ell$ only partly filled the computational domain (Figure 6). In both these simulations an initial (two dimensional) temperature profile, $T(x, y, z) = (20.0\,K)\exp(-\sqrt{x^2 + y^2}/(50.0\mathring{A}))+(20.0\,K)$, was imposed via the rescaling thermostat and let diffuse with adiabatic conditions on the lateral boundaries and periodic conditions on the top and bottom. In the case of the coupled simulation, we merely left the natural, zero flux boundary conditions in place; for the reference simulation, we imposed zero displacement boundary conditions so that no work would be done on the system and it would behave adiabatically as an NVE ensemble. Also, we used a time filter scale $\tau = 10.0\,ps$ in both simulations, which, in the case of the reference simulation, was merely used to reduce the atomic data to comparable nodal temperatures.

It is clear from the sequence of temperature contours shown in Figure 7 that the coupled simulation is quite comparable to the more computationally expensive full MD reference simulation. Figure 8 shows the normalized coarse scale energy $\sum_I \theta_I(t)/\sum_I \theta_I(0)$ for the two systems. Note that this quantity is different from the total energy expressed in Eqn. (17), since (17) uses kinetic and potential energies of the atoms in the MD region and is exactly conserved by design. Instead, the quantity plotted in Figure 8 uses the nodal temperature values everywhere in the domain; this is related to the only the kinetic energy for the atoms, and thus is not exactly conserved. In both systems, this quantity changes slightly early in the simulation; this can be attributed to the fact that the system is initially not in equilibrium and does not have an equilibrium equipartition between potential and kinetic energy. In both systems the integrated energy eventually fluctuates around a constant value; fluctuations are larger in the reference system because it contains many more atoms (131,072 vs. 32,768). The fact that our coupled system reaches a constant energy demonstrates that the method for this problem is stable, and that energy neither grows nor is dissipated by our numerical treatment.

7.3 Thermal Transport Across an Acoustic Mismatch

This example uses the same material system as in the previous examples except atoms in a two lattice unit wide region in the middle of the a computational domain $(40 \times 12 \times 12)\ell$ were given atomic masses ten times their

nominal value $10m_\alpha$ to create an ersatz grain boundary (Figure 9). As in the one-dimensional conduction simulation in Section 7.1 , lateral boundaries were prescribed to be periodic and temperatures were specified on the ends. In this case, the MD system was initially thermalized to $30\,K$ and the nodes on the left end of the computational domain were given a constant temperature of $50\,K$ and those on the right end a constant temperature of $10\,K$. A parameter study was done to show how the MD system size $(2a \times 12 \times 12)\ell$ affects the calculated temperature profile. As can be seen in Figure 10, the MD/FE boundary can be brought within three lattice units of the mismatch boundary with no substantial effect on the steady-state temperature profile. It is interesting to note that the profile is not entirely symmetric, with the low temperature side showing greater deviations across MD system size and an ordering of this difference with a. Despite this small effect, it is clear that the coupled method was successful in simulating the temperature jump expected at a grain-like boundary.

8 Discussion and Conclusions

In this work we have presented a seamless, energy-conserving method to couple the temperature fields of atomistic and continuum representations of material. The method allows the use of MD in a localized region of a domain, surrounded and overlaid by a continuum finite element solution. Inside the MD region the dynamics are governed by the detailed interatomic interactions, while everywhere else the heat transfer is governed by the Fourier heat law. A strength of the method is that computations do not depend on the boundaries of the MD region aligning with finite element faces, so that the shape of the MD region can be arbitrary. This simplifies the task of generating discretized domains; and it allows for the possibility of very simple resizing or rediscretization of both the finite element mesh and the MD lattice, which is one component of an adaptive simulation.

The main motivation for development of this method is to simulate problems in which either heat is generated in a localized region (e.g. laser heating, surface friction) or in which localized microstructures at the atomic scale strongly affect the heat transfer (e.g. thermal transport across grain boundaries or near defects). The example problem presented in Section 7.3 is an example of the latter type of application. In both cases the method can allow solution on a much larger domain than would be possible using MD alone, since MD can be used only where necessary to correctly capture the relevant phenomena. However, the method is also useful in smaller problems as a convenient way of applying temperature boundary conditions to non-equilibrium MD simulations. For example, in the example problems presented in both Sections 7.1 and 7.3 the method was used to fix the temperature on the ends of the domain;

this is an attractive alternative to other approaches that may be used, such as applying MD thermostats to regions near the boundaries which typically creates artificial Kapitza-like temperature jumps.

It should be pointed out that although we have assumed a Fourier heat law applies in the continuum region, this assumption is not required for the method presented. It is straightforward to replace Eqn. (1) with a different form, for example, the Maxwell-Cattaneo-Vernotte model typically employed to represent the finite speed of propagation of heat waves, see, e.g., [32,30,31]. On the other hand, the method does not provide an *a priori* way of determining what the correct form of the heat law should be in the continuum, nor does it allow for the analytical derivation of coefficients in a heat law. Physical or numerical experiments, or theory, must be used to provide a relation between heat flux and temperature.

A clear direction for the extension of this work is to combine the thermal coupling derived here with coupling of the momentum equations, as has been done previously using related methods, to capture the full thermo-mechanical behavior of a material. In some of this earlier work ([8], [33]) an effort has been made to eliminate internal wave reflections in the MD region caused by the discrepancy in discretization scales at the boundary. We have not concerned ourselves with this phenomenon in the current work, mainly because at finite temperatures the large number of interacting phonons de-emphasizes the importance of individual waves reflected at the boundary; reflected waves are indistinguishable from the surrounding phonons. This is in contrast to earlier work at low temperatures, for which an outgoing phonon should be removed from the domain but is not addressed by the new method presented here. However, our method does allow small-scale waves in the MD region to be tracked as thermal information as they approach the boundary, since they contribute to the nodal temperature field. Through this continuum field the small-scale energy is transported out into the continuum; this thermal information is lost if waves are removed through specialized boundary conditions as the approach the interface. Future work will focus on merging the best features of existing approaches to coupling the atomistic and continuum momentum equations with this new method for coupling the temperature fields. By combining the strengths of MD and continuum simulation methods in this way, a powerful tool can be developed for the simulation of a range of important multi-scale engineering problems.

Acknowledgments

Sandia is a multiprogram laboratory operated by Sandia Corporation, a Lockheed Martin Company, for the United States Department of Energy under con-

tract DE-AC04-94AL85000. We are grateful for helpful discussions with Rich Lehoucq, Pavel Bochev, Alex Slepoy and Jon Zimmerman in the development of this work and preparation of the manuscript.

References

[1] F. Abraham, R. Walkup, H. Gao, M. Duchaineau, T. D. la Rubia, M. Seager, Simulating materials failure by using up to one billion atoms and the world's fastest computer: Work-hardening, Proceedings of the National Academy of Sciences of the United States of America 99 (9) (2002) 5783–5787.

[2] W. Curtin, R. Miller, Atomistic/continuum coupling in computational materials science, Modelling and Simulation in Materials Science and Engineering 11 (3) (2003) R33–R68.

[3] H. Park, W. Liu, An introduction and tutorial on multiple-scale analysis in solids, Computer Methods in Applied Mechanics and Engineering 193 (17-20) (2004) 1733–1772.

[4] F. Abraham, J. Broughton, N. Bernstein, E. Kaxiras, Spanning the length scales in dynamic simulation, Computers in Physics 12 (6) (1998) 538–546.

[5] J. Knap, M. Ortiz, An analysis of the quasicontinuum method, Journal of the Mechanics and Physics of Solids 49 (9) (2001) 1899–1923.

[6] L. Dupuy, E. Tadmor, R. Miller, R. Phillips, Finite-temperature quasicontinuum: Molecular dynamics without all the atoms, Physical Review Letters 95 (6) (2005) 060202/1–4.

[7] R. Rudd, J. Broughton, Coarse-grained molecular dynamics: Nonlinear finite elements and finite temperature, Physical Review B 72 (14) (2005) 144104–1–32.

[8] G. Wagner, W. Liu, Coupling of atomistic and continuum simulations using a bridging scale decomposition, Journal of Computational Physics 190 (1) (2003) 249–274.

[9] H. Park, E. Karpov, W. Liu, A temperature equation for coupled atomistic/continuum simulations, Computer Methods in Applied Mechanics and Engineering 193 (17-20) (2004) 1713–1732.

[10] M. Muser, Towards an atomistic understanding of solid friction by computer simulations, Computer Physics Communications 146 (1) (2002) 54–62.

[11] D. Ivanov, L. Zhigilei, Combined atomistic-continuum modeling of short-pulse laser melting and disintegration of metal films, Physical Review B 68 (6) (2003) 064114.

[12] P. Gumbsch, R. Cannon, Atomistic aspects at brittle fracture, MRS Bulletin 25 (5) (2000) 15–20.

[13] M. Horstemeyer, M. Baskes, S. Plimpton, Computational nanoscale plasticity simulations using embedded atom potentials, Theoretical and Applied Fracture Mechanics 37 (1-3) (2001) 49–98.

[14] A. Maiti, G. Mahan, S. Pantelides, Dynamical simulations of nonequilibrium processes - heat flow and the Kapitza resistance across grain boundaries, Solid State Communications 102 (7) (1997) 517–521.

[15] J. Schall, C. Padgett, D. Brenner, Ad hoc continuum-atomistic thermostat for modeling heat flow in molecular dynamics simulations, Molecular Simulation 31 (4) (2005) 283–288.

[16] C. Padgett, D. Brenner, A continuum-atomistic method for incorporating Joule heating into classical molecular dynamics simulations, Molecular Simulation 31 (11) (2005) 749–757.

[17] J. Weiner, Statistical Mechanics of Elasticity, 2nd Edition, Dover, Mineola, NY, 2002.

[18] J. Casas-Vazquez, D. Jou, Nonequilibrium temperature versus local-equilibrium temperature, Physical Review E (Statistical Physics, Plasmas, Fluids, and Related Interdisciplinary Topics) 49 (2) (1994) 1040 – 8.

[19] A. Baranyai, Temperature of nonequilibrium steady-state systems, Physical Review E (Statistical Physics, Plasmas, Fluids, and Related Interdisciplinary Topics) 62 (5) (2000) 5989 – 97.

[20] E. Bertin, O. Dauchot, M. Droz, Temperature in nonequilibrium systems with conserved energy, Physical Review Letters 93 (23) (2004) 230601 – 4.

[21] C. Braga, K. P. Travis, A configurational temperature Nose-Hoover thermostat, Journal of Chemical Physics 123 (13) (2005) 134101 – 1.

[22] J. Casas-Vazquez, D. Jou, Temperature in non-equilibrium states: a review of open problems and current proposals, Reports on Progress in Physics 66 (11) (2003) 1937 – 2023.

[23] O. C. Zienkiewicz, R. L. Taylor, The Finite Element Method, 4th Edition, Vol. 1, McGraw-Hill, London, 1989.

[24] W. Hoover, Canonical dynamics - equilibrium phase-space distributions, Physical Review A 31 (3) (1985) 1695–1697.

[25] H. Berendsen, J. Postma, W. Vangunsteren, A. Dinola, J. Haak, Molecular-dynamics with coupling to an external bath, Journal of Chemical Physics 81 (8) (1984) 3684–3690.

[26] T. Ikeshoji, B. Hafskjold, Nonequilibrium molecular-dynamics calculation of heat-conduction in liquid and through liquid-gas interface, Molecular Physics 81 (2) (1994) 251–261.

[27] J. Haile, Molecular Dynamics Simulation: Elementary Methods, Wiley, New York, 1992.

[28] C. Gear, Numerical Initial Value Problems in Ordinary Differential Equations, Prentice-Hall, Englewood Cliffs, New Jersey, 1971.

[29] K. Tretiakov, S. Scandolo, Thermal conductivity of solid argon from molecular dynamics simulations, Journal of Chemical Physics 120 (8) (2004) 3765–3769.

[30] S. Volz, J. B. Saulnier, M. Lallemand, B. Perrin, P. Depondt, M. Mareschal, Transient Fourier-law deviation by molecular dynamics in solid argon, Physical Review B (Condensed Matter) 54 (1) (1996) 340 – 7.

[31] J.-R. Ho, C.-J. Twu, C.-C. Hwang, Molecular-dynamics simulation of thermoelastic waves in a solid induced by a strong impulse energy., Physical Review B (Condensed Matter and Materials Physics) 64 (1) (2001) 014302 – 10.

[32] D. D. Joseph, L. Preziosi, Heat waves, Reviews of Modern Physics 61 (1) (1989) 41 – 73.

[33] X. Li, W. E, Variational boundary conditions for molecular dynamics simulations of solids at low temperature, Communications in Computational Physics 1 (1) (2006) 135–175.

List of Figures

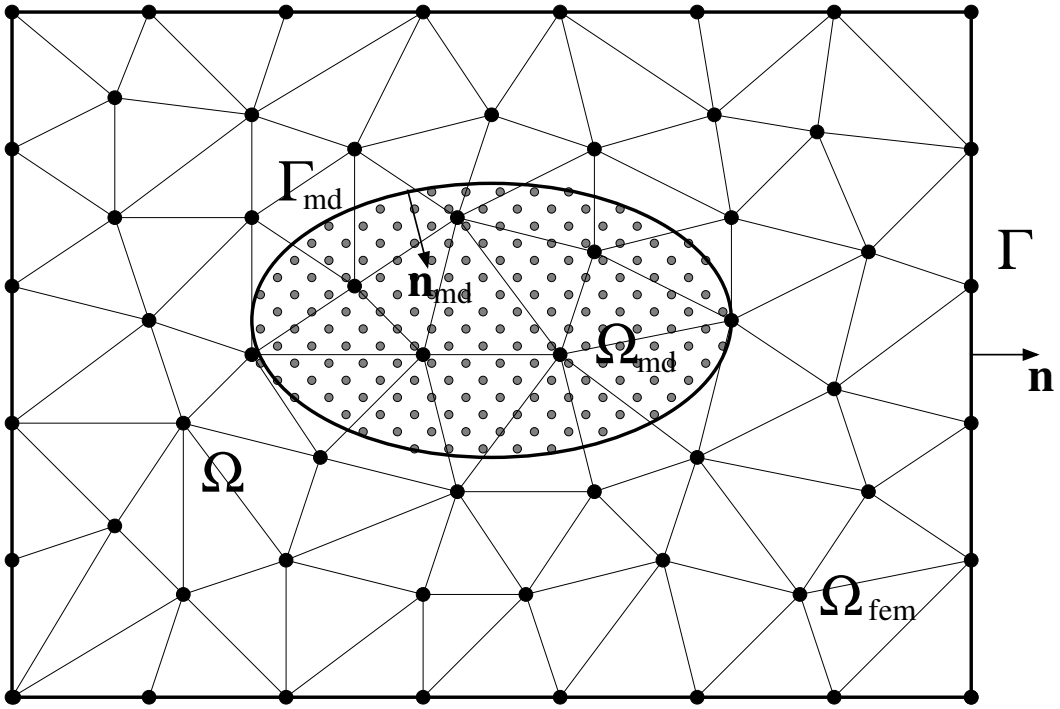

Fig. 1. Coupled domain geometry

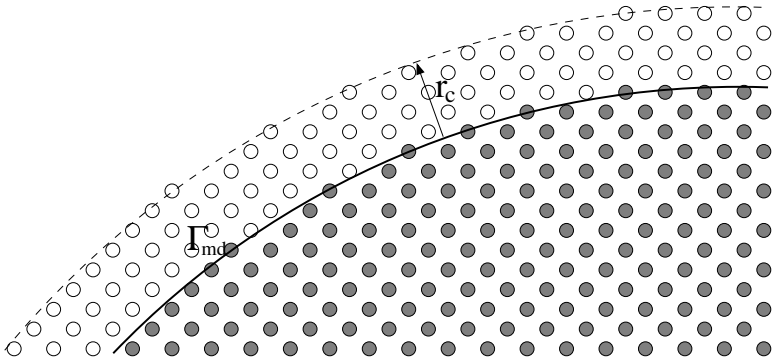

Fig. 2. Ghost atoms (empty circles) near Γ_{md} used to compute interatomic forces.

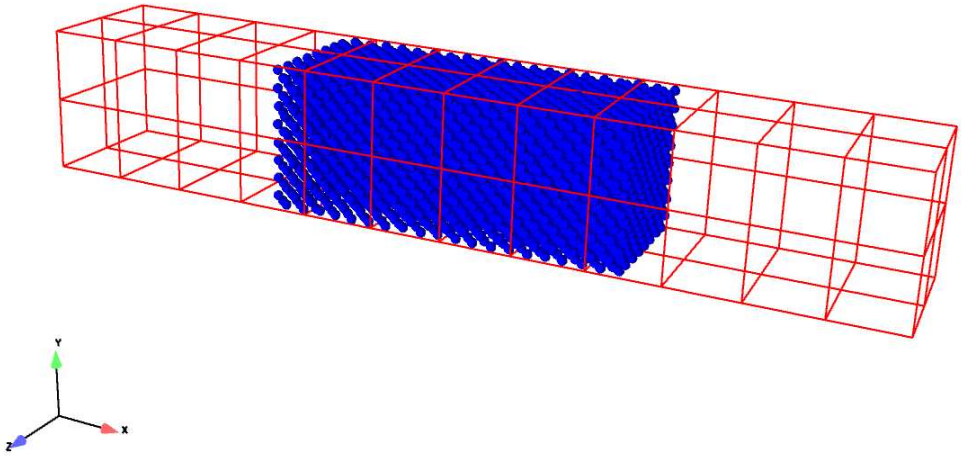

Fig. 3. One dimensional heat conduction: mesh and atomic positions for $h = 4\ell$

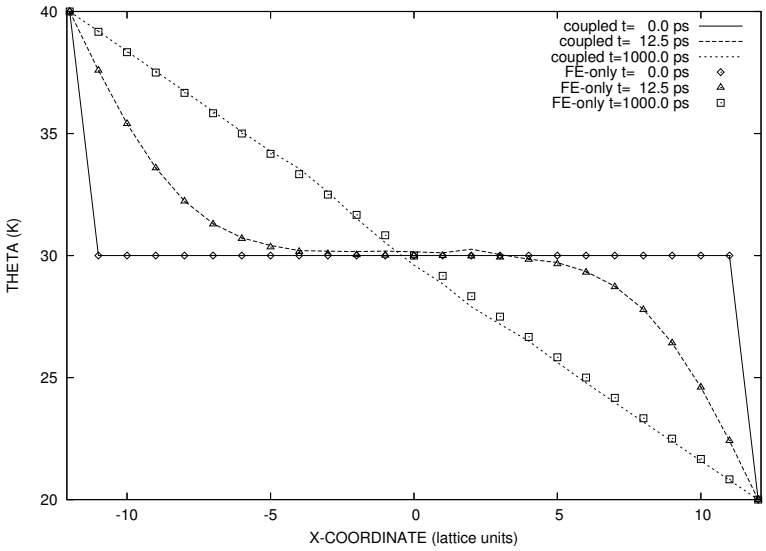

Fig. 4. Temperature profiles for $h = 2\ell$ and $\tau = 25\,ps$ at $t = 0.0,\ 12.5,\ 1000.0\,ps$

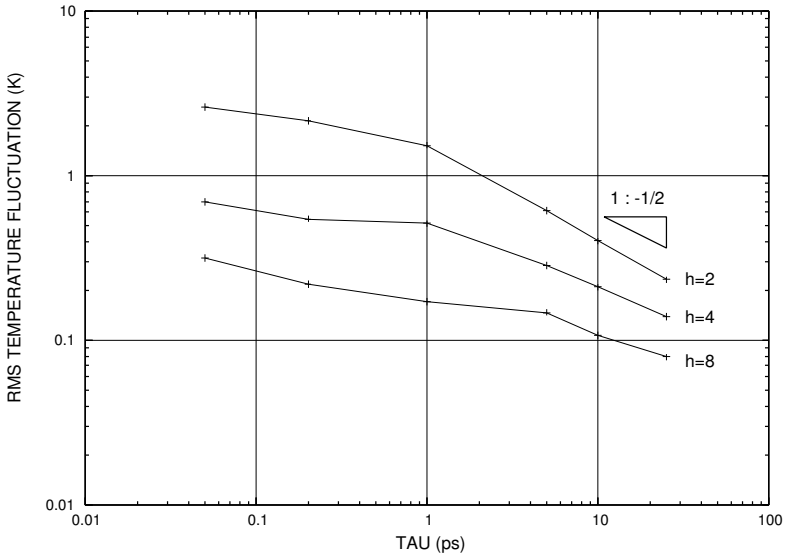

Fig. 5. Root mean square fluctuations of temperature at center of the domain as a function of τ for various h

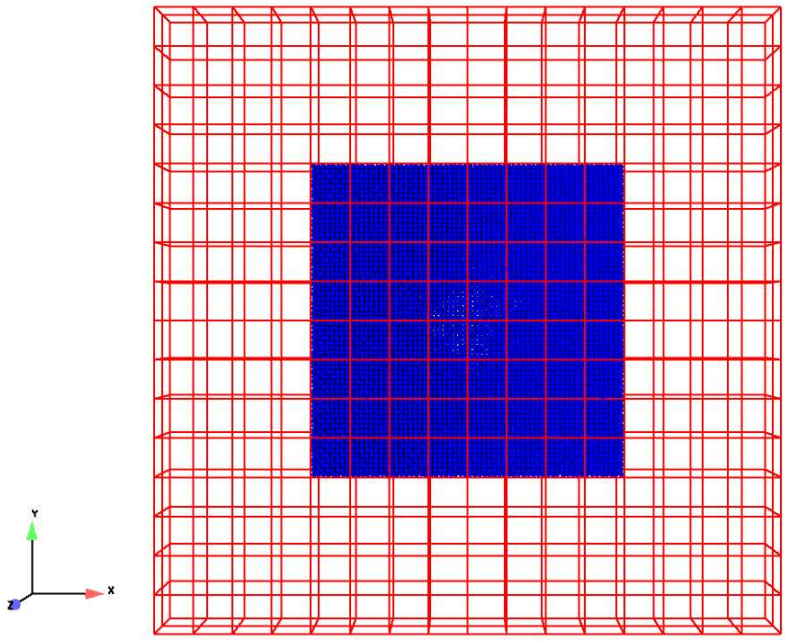

Fig. 6. Mesh and atomic positions for the coupled simulation of the diffusion of an initial Gaussian temperature profile

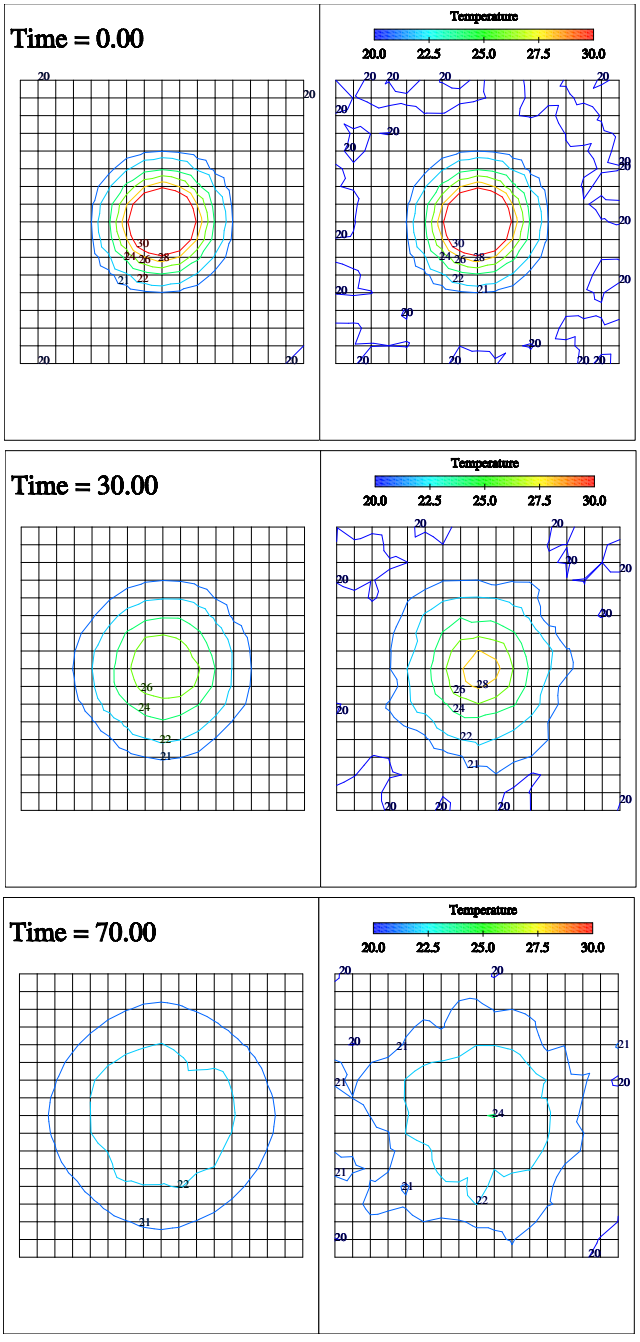

Fig. 7. Comparison of a sequence of temperature contours for the coupled simulation (left) and the reference simulation (right): (a) initial $t = 0.0\,ps$, (b) $t = 30.0\,ps$, and (c) $t = 70.0\,ps$

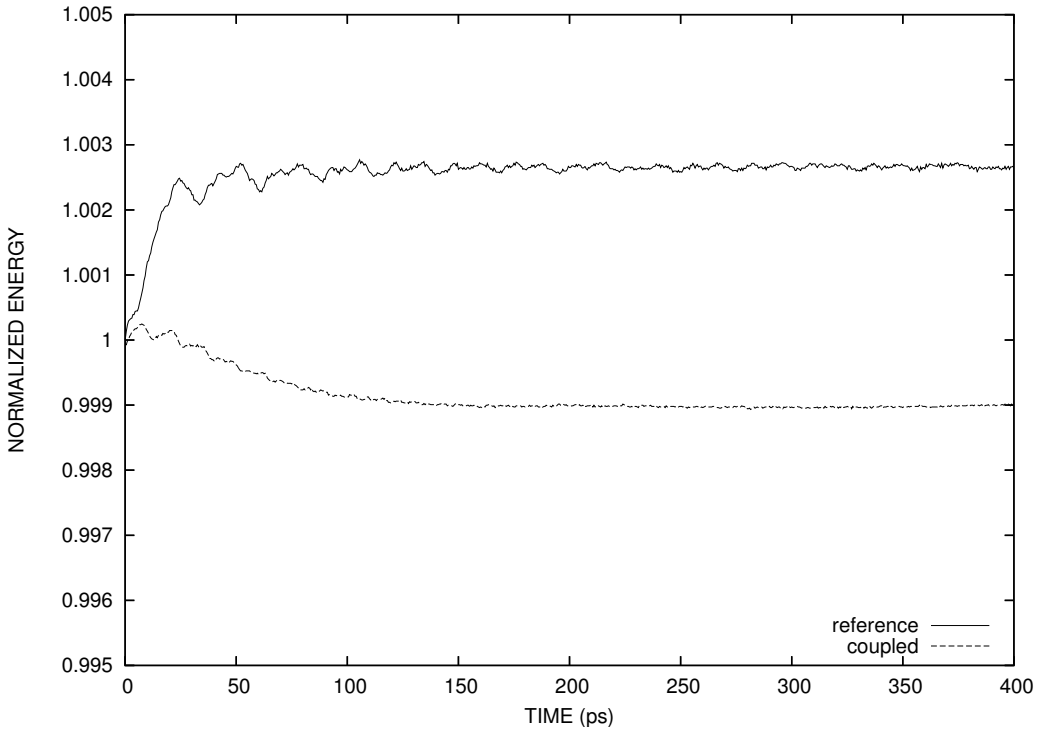

Fig. 8. Comparison of integrated temperature evolution for the diffusion of a Gaussian temperature profile

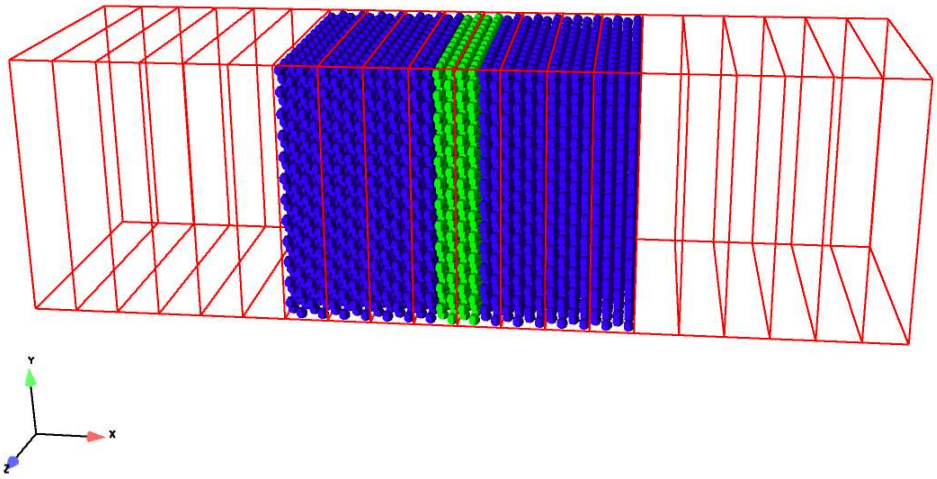

Fig. 9. Mesh and atomic positions for $a = 8$ showing regions of different atomic mass (blue: atoms with normal mass, green: heavy atoms in the center of simulation)

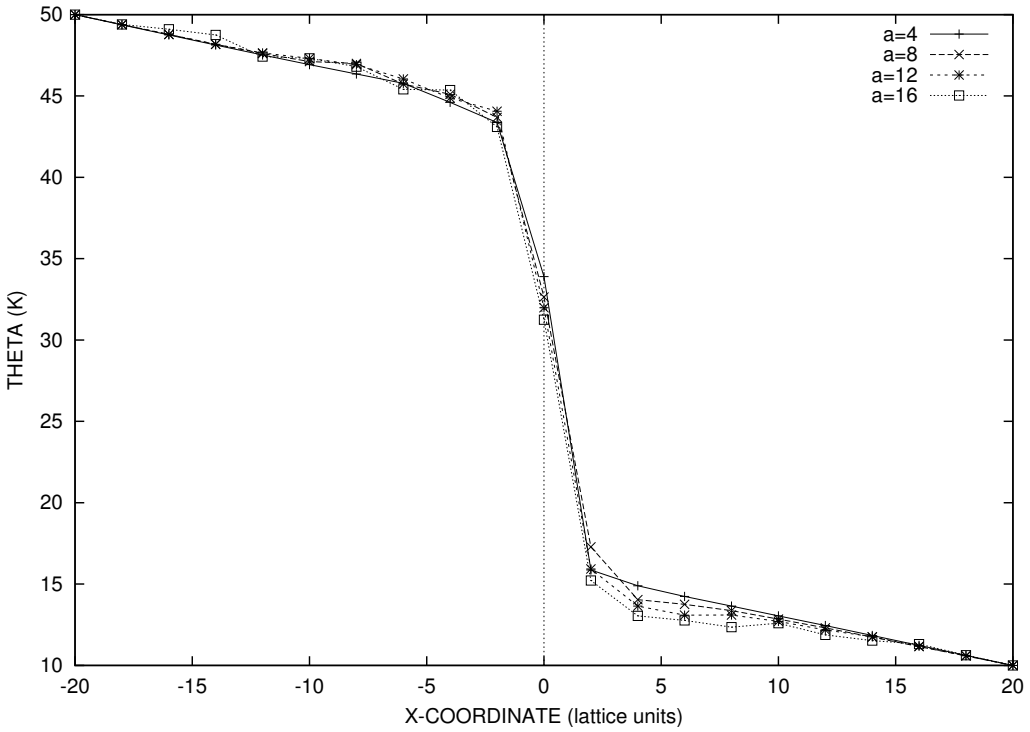

Fig. 10. Temperature profiles for various atomic domain sizes a